JOURNAL OF MATERIALS SCIENCE 37 (2002) 5065–5073

On the effects of thermomechanical processing on failure mode in precipitation-hardened aluminium alloys

M. DE HAAS, J. TH. M. DE HOSSON
Department of Applied Physics, Materials Science Centre and Netherlands Institute for Metals Research, University of Groningen, Nijenborgh 4, 9747 AG Groningen, The Netherlands
E-mail: hossonj@phys.rug.nl

This paper concentrates on the influences of thermomechanical processing on fracture behaviour of Al-Mg-Si-Cu (AA6061) alloys. Important factors are grain boundary structure and extent of matrix- and grain boundary precipitation. Large grain boundary phases in the as-air-cooled alloy, explains its much smaller fracture strain with respect to the water-quenched alloy. With increasing artificial ageing time, the bulk fracture strain of the air-cooled alloy exhibits a minimum. This is due to grain boundary precipitate growth and coarsening affecting the fraction of strain confined to the grain boundary region. For the recrystallized microstructure aged to peak strength, the fraction of intergranular fracture is much larger for the air-cooled alloy. This can be understood on the basis of a much wider precipitate free zone and a smaller grain boundary precipitate volume fraction for the air-cooled alloy, increasing the fraction of strain confined to the grain boundary region by about one order of magnitude with respect to the water-quenched alloy. A much coarser distribution of intermetallic phases in the extruded microstructure is responsible for a larger degree of slip localization. This enhances the tendency for shear- and intergranular fracture, reducing the ductility and thus the fracture strain with respect to that of the recrystallized microstructure.

1. Introduction

The heat-treatable Al-Mg-Si-Cu (AA6061) alloy finds wide application as construction material in the transportation and building industry markets. The main advantage of these aluminium alloys is their high specific strength. However, commercial applications may be limited by poor characteristics such as a lower fracture toughness which is known to depend on many parameters, e.g., intermetallic content, grain size and grain boundary structure [1, 2]. In the present study, the influences of thermomechanical processing on fracture mechanics have been considered. Important factors are grain boundary structure and extent of matrix- and grain boundary precipitation. Overall, it is recognized that varying microstructural conditions may favour different combinations of failure modes in medium- and high-strength aluminium alloys.

2. Fracture strain in relation to grain boundary precipitation

During an isothermal ageing sequence, many precipitation-hardening alloys exhibit a condition in which the interior of the grains is highly hardened while the grain boundary environment remains very soft (i.e., the precipitate free zone or PFZ). This softness finds its origin in a local depletion of vacancies and solute inhibiting the formation of a fine dispersion of particles in that region. Experiments indicate that the plastic strain can be highly localized inside these soft zones and that the interface between precipitate and matrix acts as a preferred site for initiation and propagation of cracks. In this way the alloy may fail according to an intergranular but ductile mechanism. When the grain interior and grain boundary region are of comparable hardness, concentration of strain at the grain boundary region is not pronounced and a more transgranular type of fracture is prevalent. Fig. 1 schematically depicts these different modes of failure.

Considered that in most precipitation hardening alloys incoherent precipitates form by heterogeneous nucleation at grain boundaries, it can be expected that their local volume fraction f_i will lower the fracture strain ε_{fi} that is confined to the grain boundary region according to [3, 4]:

$$\varepsilon_{fi} = \left(\sqrt{\frac{\pi}{6 f_i}} - \sqrt{\frac{2}{3}} + \varepsilon_n \right)^{\frac{1}{C}} - 1 \qquad (1)$$

where $C \sim 1.5$ is a factor accounting for the faster extension rate of voids as compared to the matrix before the critical condition of instability is reached, ε_n is a critical strain to nucleate a void at the interface of an incoherent particle and f_i is the volume fraction of grain boundary precipitates acting as void nuclei. The failure

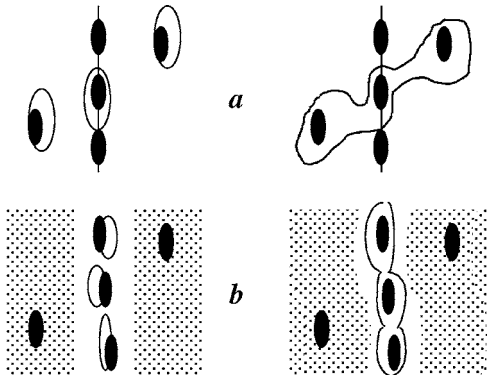

Figure 1 Schematic representation of failure mechanisms in precipitation hardened alloys (a) No localization of strain at the grain boundary (b) Localization of strain at the grain boundary.

strain corresponds to the strain necessary to extend the voids up to a length equal to the particle spacing. When this point is reached, fracture will occur along the grain boundary. In addition, the bulk strain to fracture ε_f (without a pre-crack) depends on the grain size D and the PFZ-width d according to [5]:

$$\varepsilon_f = \varepsilon_{ft} + \varepsilon_{fi}\frac{d}{D} \tag{2}$$

where ε_{ft} is the portion of transcrystalline strain. The critical value which determines ε_f can then be either ε_{ft} or ε_{fi}, which in turn depends on the difference in critical shear stress inside the PFZ and the grain interior, and therefore on the ageing condition.

If all strain is confined in the soft grain boundary environment, the first term on the right-hand side of the equation can be neglected. The above equation is valid when the assumption is made that $d \ll D$, which holds for the alloys investigated in this work.

An important parameter governing grain boundary precipitation is the applied cooling-rate after the alloy has been solution heat treated. It is well known that slack quenches reduce toughness, especially in recrystallized microstructures, because of the much larger fraction of random high angle grain boundaries. The precipitates tend to be smaller on low-angle grain boundaries, because of the smaller solute diffusivity that leads to a slower precipitate growth rate. The precipitate-free-zones that circumvent these boundaries are smaller as well. In addition, sub grain boundaries have a much higher cohesive strength than high angle grain boundaries, arising from the nature of the grain boundary itself as well as the nature of the interface of the boundary precipitates. Planar slip is expected to traverse more easily the sub-boundaries because of their small angle of misorientation, which may reduce large stress concentrations at the head of piled-up dislocations. Thus, the high-angle grain boundaries will be most susceptible to crack propagation, as the work needed to advance along them will be less than along low-angle grain boundaries [6].

3. Processing routes

For the present study, aluminium alloy 6061 was used. This alloy contains 1.0 at% Mg, 0.7 at% Si, 0.15 at% Cu for precipitation hardening and 0.25 at% Fe, 0.15 at% Cr and 0.06 at% Mn for formation of intermetallic phases. From the as-received (as-extruded) state, two alternative processing routes were applied and these are schematically depicted in Fig. 2:

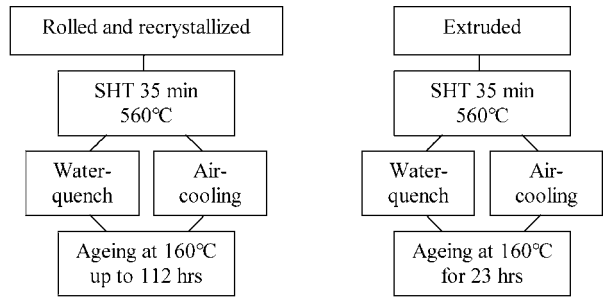

Figure 2 Applied thermomechanical processing routes.

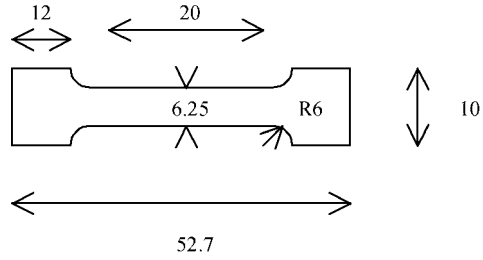

Figure 3 Tensile specimen with dimensions in mm (thickness: 1.3 mm).

1. To obtain a recrystallized microstructure, it was cold-rolled with intermediate annealing treatments at 560°C such that the last rolling step realized a reduction of ∼30%. From the rolled plate, with a thickness of 1.3 mm, tensile specimens were laser-cut according to the dimensions of Fig. 3. Each specimen was given an annealing treatment for 35 minutes at 560°C and was subsequently either water-quenched or air-cooled. Finally, all samples were artificially aged at 160°C for times ranging up to 112 hrs. Samples aged for 3 minutes at 160°C will be referred to as "as-quenched" from now on. This treatment is applied in order to stabilize the as-cooled alloy [7]. Both water-quenched and air-cooled alloys have a random distribution of grain boundary plane orientations, because they consist of equiaxed grains.

2. To preserve the extruded microstructure, plates perpendicular to the extrusion direction with a thickness of 1.3 mm were sawn. Subsequently, the tensile specimens were laser-cut. Every specimen was given an annealing treatment for 35 minutes at 560°C and was subsequently either water-quenched or air-cooled. Finally, an artificial ageing treatment at 160°C for 23 hrs was applied. After this treatment, the typical texture for extruded product was found to be still present. The distribution of the intermetallic phases in this microstructure is found to be much coarser than for the rolled and recrystallized microstructure.

For both processing routes, additional samples for investigation by orientation-imaging microscopy (OIM) or transmission electron microscopy (TEM) were prepared as well.

In this work, all tensile tests were performed at an elongation rate of 10 μm s^{-1}, using a gage length of 20 mm, which resulted in a strain rate of 5.0×10^{-4} s^{-1}.

4. Results

The stress-strain curves of both water-quenched and air-cooled recrystallized alloys are depicted in Fig. 4a and b respectively for different times of artificial ageing at 160°C. Each curve is the average of two independent measurements. From Fig. 4a, it can be seen that for the water-quenched alloy the strength first increases up to the point of peak strength (at 23 hrs) and subsequently decreases again with ageing time (i.e., over-ageing). The fracture strain monotonically decreases with ageing time. These observations are to be expected for precipitation-hardened alloys. The strength of the air-cooled alloy, although smaller in magnitude, shows the same trend with ageing time as that of water-quenched product. The interesting part however, is the fracture strain, which first exhibits a local minimum at about 5 hrs of ageing before increasing again to a next local maximum somewhere in the range 22 hrs–112 hrs.

Extruded material, water-quenched or air-cooled, was aged for 23 hrs at 160°C and tested in tension at the same strain rate. The stress-strain curves, which are again the average of two independent measurements, are depicted in Fig. 5. The aged samples of the extruded material followed the same trend as shown by the recrystallized alloys (re the trend shown in Fig. 4). The difference in strength between the water-quenched and air-cooled alloys is comparable to that of the recrystallized microstructure, whereas the fracture strain can be seen to be much smaller than that of the recrystallized product. Also a large fracture strain difference

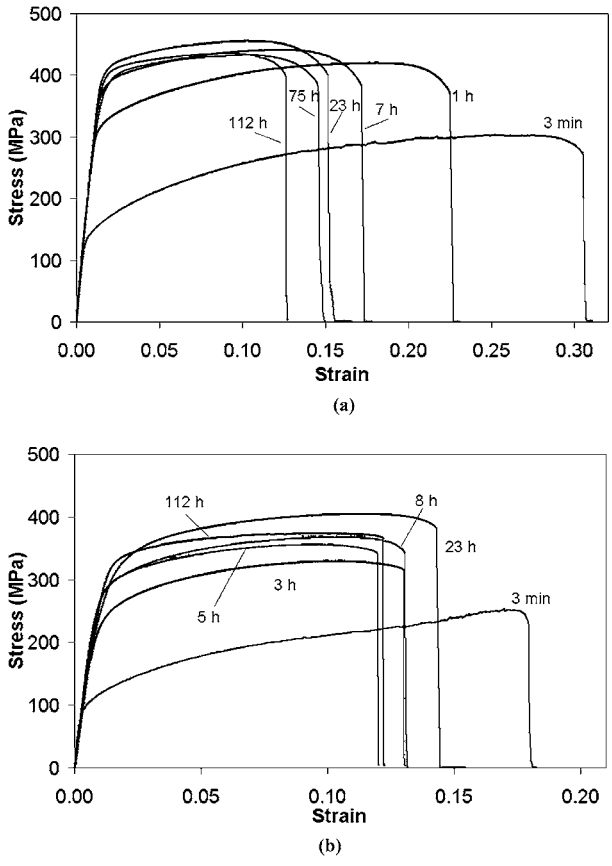

Figure 4 Stress-strain diagrams of AA6061 with recrystallized microstructure at different states of artificial ageing. (a) Water quenched and (b) Air-cooled.

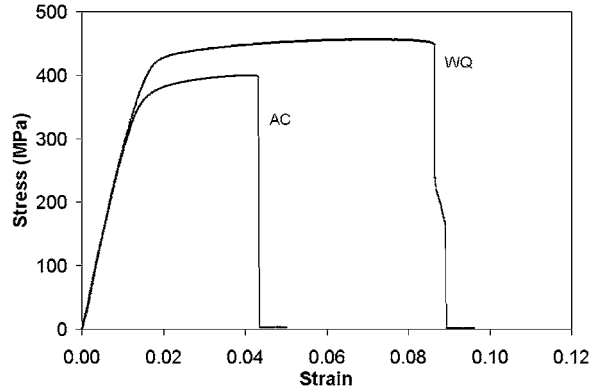

Figure 5 Stress-strain diagrams of AA6061 with extruded microstructure subjected to different cooling rates WQ—water quenched, AC—air-cooled.

(∼4.5%) between the water-quenched and air-cooled alloy is evident.

After the samples were tested in tension, their fracture surface was examined in a scanning electron microscope. To obtain better insight into the fracture mechanism of both water-quenched and air-cooled alloy after different times of artificial ageing at 160°C, the fracture surfaces of samples in underaged, peak-aged and overaged conditions are compared in Fig. 6.

For the recrystallized water-quenched alloy, the uniform strain to fracture monotonically decreases during ageing, but the ductility (as measured from the aspect of the fracture surfaces) first increases from the underaged to the peak-aged state and then decreases again in the over-aged microstructure (Fig. 6a–c). The fracture mode is mainly transgranular and the fraction of intergranular fracture is largest in the peak-aged condition. As can be seen in Fig. 6a, for the under-aged alloy, relatively flat shear zones connect the dimples. As ageing proceeds the fracture surface between the large dimples becomes covered by smaller dimples. Also the portion of intergranular failure increases (Fig. 6b) because the difference in yield stress between grain boundary region and grain interior increases accordingly. As grain size and distribution of the intermetallic phases both remain unaltered during artificial ageing, the change in mechanical response can be attributed solely to changes in matrix- and grain boundary precipitation. In the underaged state, the thin needle-shaped precipitates in the matrix are easily cut by moving dislocations, leading to an effective softening of slip planes and the consequent formation of intense slip bands, which favours shearing. On the contrary, in the peak-aged condition a significant proportion of the needles is by-passed by an Orowan mechanism and the resistance to shearing is increased, which enhances ductility. As matrix precipitation coarsens during over-aging, the tendency for shearing increases again, which is evident from Fig. 6c. Here the fracture surface consists mainly of flat shear zone and regions of intergranular failure.

From Fig. 6d it can be observed that the fracture mechanism of the unaged air-cooled sample is predominantly of a ductile transgranular type with regions of shear, whereas the 23 hrs aged sample seems to have failed mainly according to a ductile intergranular

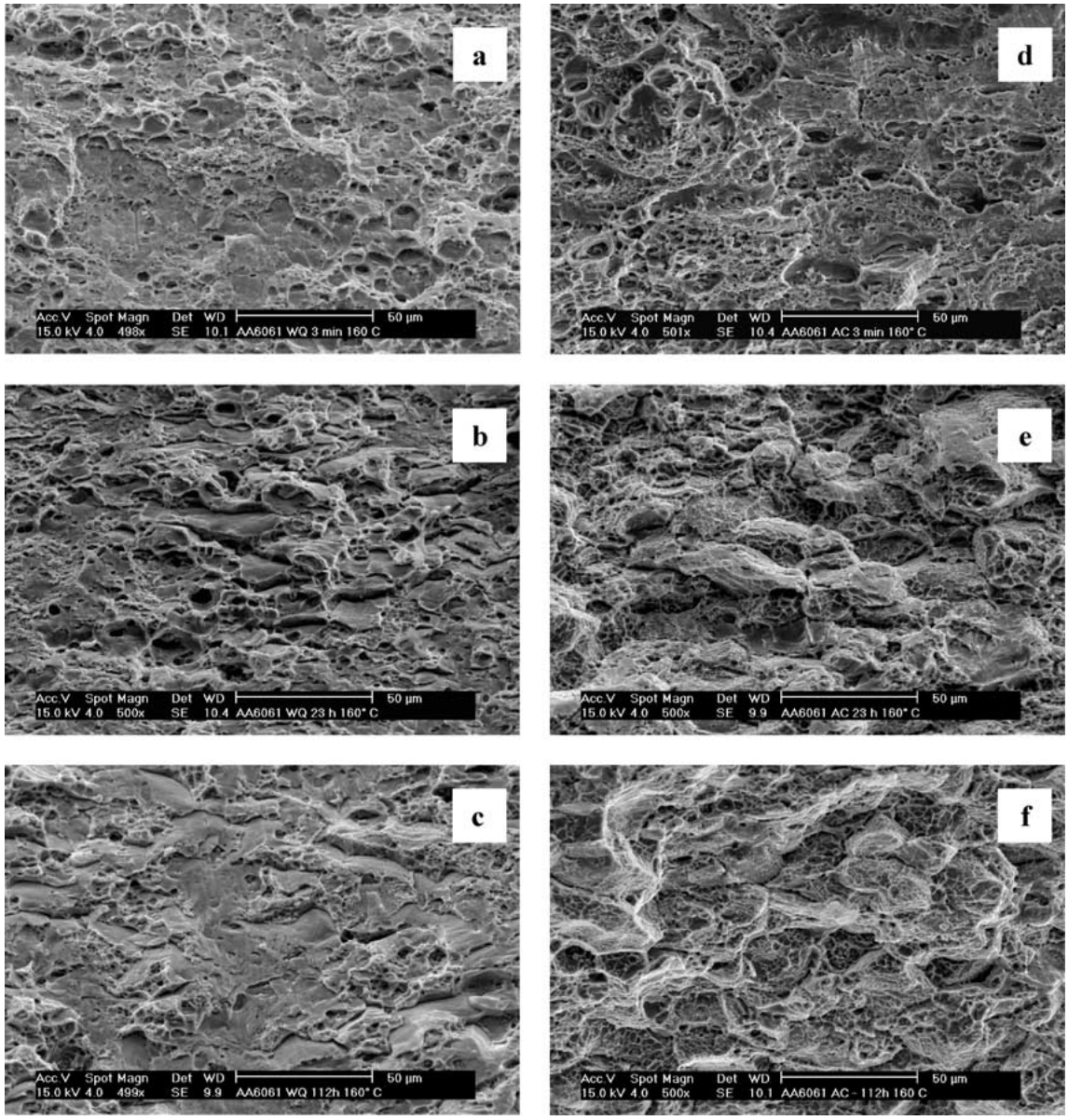

Figure 6 Fracture surfaces (500×) of rolled and recrystallized AA6061 water-quenched (WQ) or air-cooled (AC) and subsequently aged at 160°C for different times (a) WQ, 3 min; (b) WQ, 23 h; (c) WQ, 112 h; (d) AC, 3 min; (e) AC, 23 h; (f) AC, 112 h.

fracture mode (Fig. 6e). Apparently, a transition from ductile transgranular- to ductile intergranular fracture mode sets in with artificial ageing time, which can be explained by the increase in yield stress difference between grain boundary zone and grain interior with ageing time until peak-strength is achieved. In this way plastic deformation may become located to a larger degree at the relatively soft grain boundary region. For the overaged state (Fig. 6f), the fraction of intergranular failure has slightly decreased again.

As mentioned earlier, the influence of the properties of the grain boundary region on fracture strain is largest when the difference between yield stress of grain boundary region and grain interior is largest (i.e., in the peak-aged condition). The concentration of plastic deformation in the grain boundary region will then be largest. In Fig. 7a and b respectively the fracture surfaces of water-quenched and air-cooled alloys in peak-aged condition (i.e., 23 hrs at 160°C) are compared at high magnification. The amount of plastic deformation in the grain boundary region (as measured by cusp-depth) can clearly be seen to be much smaller for the water-quenched case.

Samples consisting of an extruded microstructure at peak-strength were tested in tension in the same way as the rolled and recrystallized samples. Comparing Fig. 8a–c vs. 8d–f, it can be seen that grain boundary cusp-size and –depth are largest for the air-cooled alloy just as was observed for the rolled and recrystallized alloy. Most probably, both parts depicted in these figures are the results of fracture at random high-angle grain boundaries. The fraction of intergranular failure for both cooling rates is notably smaller than for the recrystallized microstructure aged to the same condition. Because of the coarser distribution of intermetallic phase in the grain interior of the extruded microstructure, the degree of slip localization is larger, from which a larger portion of intergranular fracture may be expected. The observation that it is actually smaller can be interpreted as additional support for the large resistance of the low-angle grain boundaries to intergranular failure.

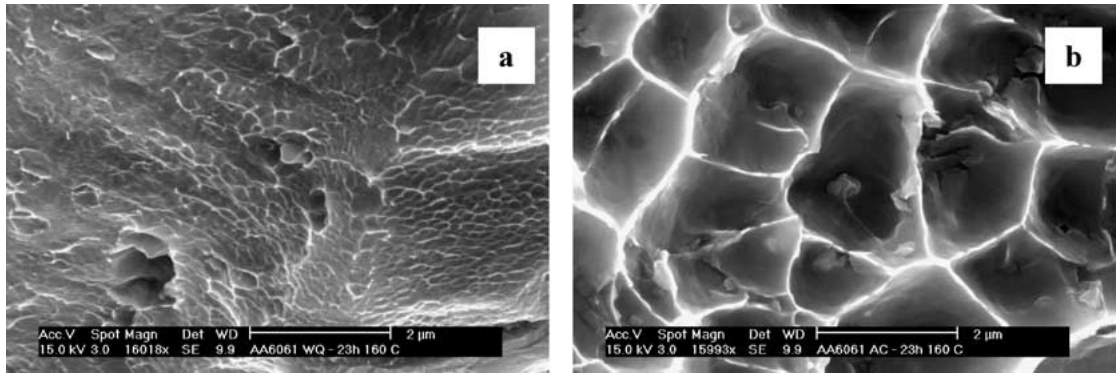

Figure 7 Fracture surfaces of rolled and recrystallized AA6061 water-quenched (WQ) or air-cooled (AC) and subsequently aged to peak strength (23 h at 160°C) (a) WQ, 16000x; (b) AC, 16000x.

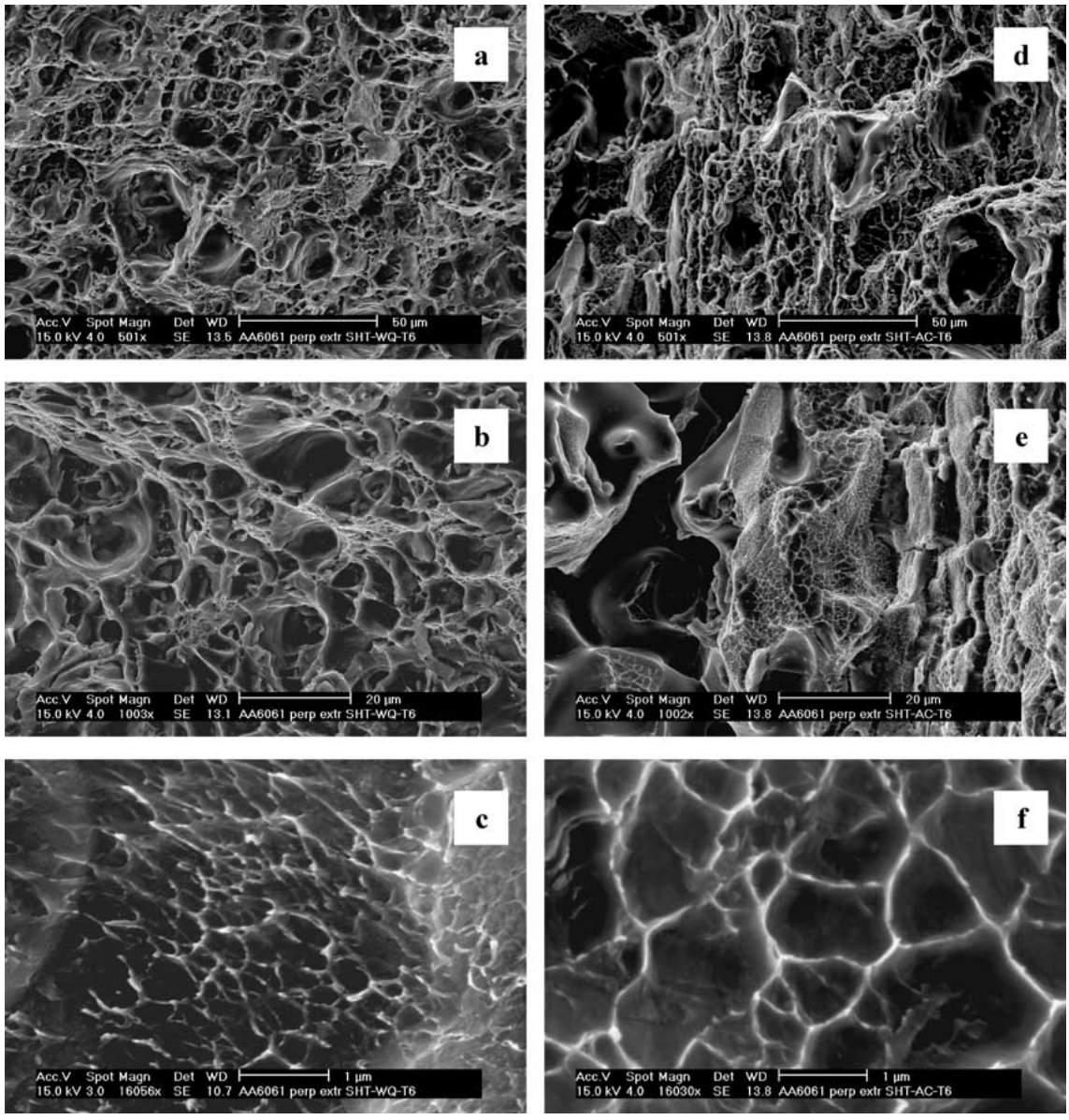

Figure 8 Fracture surfaces of extruded AA6061 water-quenched (WQ) or air-cooled (AC) and subsequently aged to peak strength (23 h at 160°C) (a) WQ, 500x; (b) WQ, 1000x; (c) WQ, 16000x; (d) AC, 500x; (e) AC, 1000x; (f) AC, 16000x.

In Fig. 9a and b transmission electron micrographs of an air-cooled sample aged to peak-strength are presented. These figures give a reasonable indication for the precipitate size and inter-distance at random high-angle grain boundaries in air-cooled alloy. The size varies between 0.5 μm and 2 μm and the centre-to-centre distance between the phases is about 0.7 μm, which compares to the sizes of the dimples observed on top of the intergranular facets ($\sim$1–2 μm). Comparing Fig. 9a and c, the width of the precipitate-free-zones around random high-angle grain boundaries can be determined to be about 35 nm and 280 nm for

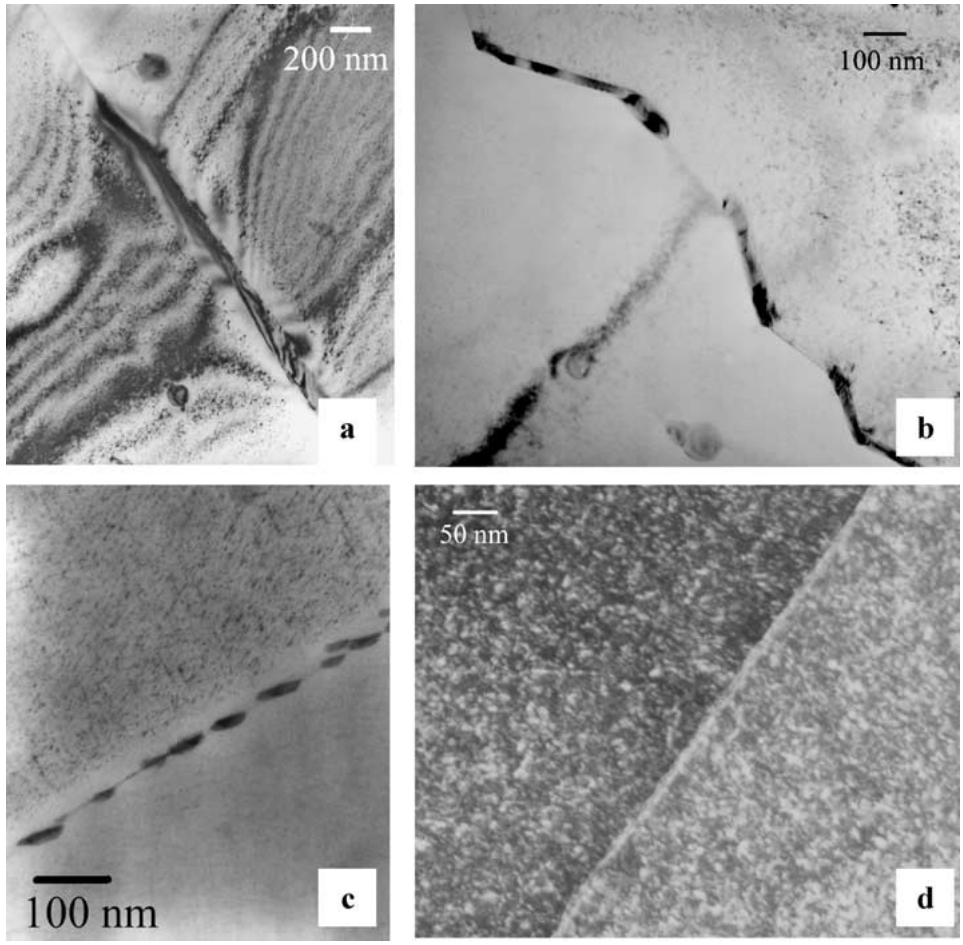

Figure 9 Grain boundary precipitation and PFZ-widths in AA6061. (a,b) Recrystallized, Air-cooled, aged 23 hrs at 160°C, general GB. (c) Recrystallized, Water-quenched, aged 50 hrs at 160°C, general GB. (d) Extruded, Water-quenched, aged 23 hrs at 160°C. Low-angle grain boundary (5° on a [111]), Dark-field image.

the water-quenched and air-cooled alloys, respectively. Fig. 9d depicts a dark-field micrograph of a low-angle (5° on a [111]) grain boundary in extruded product aged to peak strength. Precipitation is not resolved and the width of the precipitate-free-zone is negligible, indicating a very small amount of solute-vacancy segregation to this grain boundary during the quench.

5. Discussion

5.1. Recrystallized microstructure

As the fracture mode of both water-quenched and air-cooled material without artificial ageing is mainly transgranular, the fracture strain cannot directly be related to precipitation at grain boundaries or grain boundary fracture energy. The fracture mechanism can be described by initiation of voids at the interfaces between the intermetallic phases and the matrix. As can be observed comparing Fig. 4a and b, the fracture strain for the as-air-cooled alloy is much smaller than for the as-water-quenched sample (i.e., 18% vs. 31%). Since both the grain size and the size and distribution of the matrix intermetallic phases in both alloys are comparable (i.e., apart from cooling rate they were both subjected to the same processing route), the only differences are heterogeneous precipitate nucleation at the intermetallics in the matrix and extensive grain boundary precipitation for the air-cooled alloy. As the first difference should only have a decreasing effect on matrix slip localization and thus on the tendency for shear- or intergranular fracture, the second difference is most likely to be responsible for the smaller fracture strain. Although fracture is not of intergranular type, large grain boundary phases nucleated during air-cooling, can assist in void formation and in linkage of voids that nucleated at intermetallic phases within the interior of the grains (schematically depicted in Fig. 10). Consequently, the fracture strain may be reduced significantly.

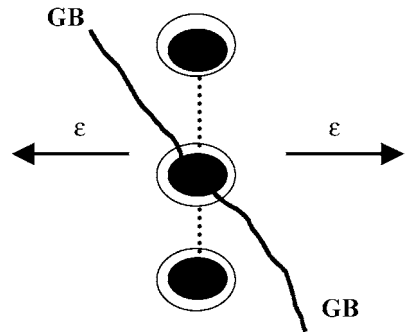

Figure 10 Void nucleated at grain boundary phase may assist in link-up of voids nucleated at matrix phases.

Fig. 11a depicts the fracture energy determined by integrating the area under the stress-strain curves in the plastic regime. From this figure it can be seen that the fracture energy for the air-cooled alloy first increases slightly with ageing time, just as for the water quenched

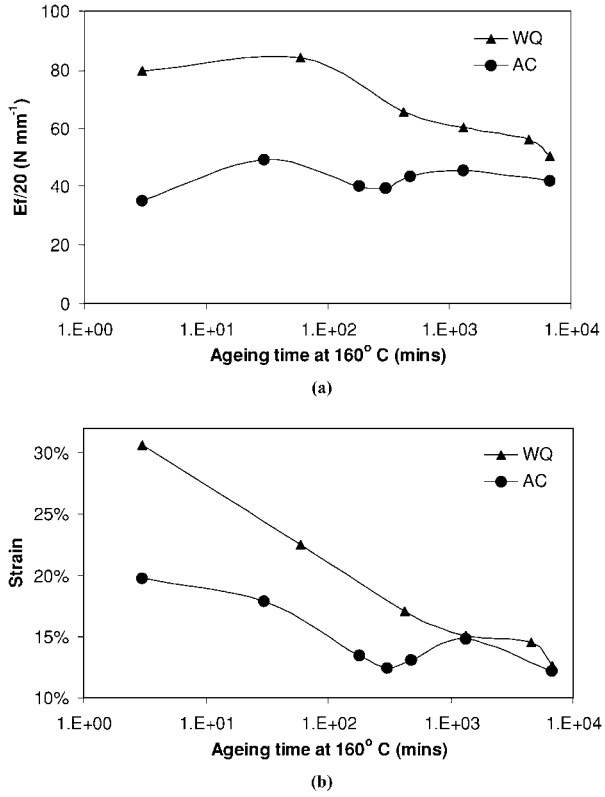

Figure 11 Mechanical response of water-quenched (WQ) and air-cooled (AC) AA6061 alloy. (a) Fracture energy against artificial ageing time at 160°C and (b) fracture strain against artificial ageing time at 160°C.

case. This initial rise is mainly the result of an increase in yield stress. Starting from the point of maximum fracture energy, a significant difference between the water-quenched and the air-cooled alloy is apparent; the fracture energy of the water-quenched alloy further decreases with ageing time, whereas for the air-cooled alloy it first decreases, reaches a local minimum after about 5 hrs of ageing and then increases again to a next local maximum. When only the fracture strain is plotted against ageing time (Fig. 11b), it can be observed that, except for underaged state, the shape of the fracture energy curve of both alloys is mainly affected by the fracture strain. For the air-cooled case, this strain is predominantly controlled by grain boundary properties in a broad range around the peak-aged condition. This can be validated when the fracture surfaces of the air-cooled alloy for different times of ageing are considered (Fig. 6d–f). Here it can be observed that, except for the extreme underaged case, the fracture mode is predominantly of ductile intergranular nature, whereas for the water-quenched alloy a larger portion of transgranular fracture is observed. For the air-cooled alloy, a larger degree of correlation thus exists between bulk fracture energy and the properties of the grain boundary region, explaining the observed difference in trend in fracture energy for the two cooling-rates.

The observed trend for the fracture strain of the air-cooled alloy can be explained by grain boundary fractional area coverage with precipitates. During the first stages of ageing, the grain boundary precipitates slightly grow, aided by both the remaining grain boundary solute-concentration and the solute-supply from the grain interior. Because of precipitate growth, the fractional area coverage increases slightly and from

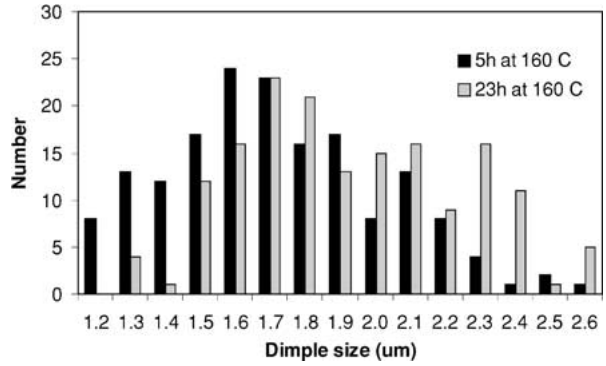

Figure 12 Cusp size distributions for air-cooled product artificially aged for times of 5 hrs and 23 hrs at 160°C.

Equation 1 it can be seen that this will decrease the local (i.e., confined to the soft grain boundary region) critical fracture strain. The bulk fracture strain will then also decrease according to Equation 2, because the portion of transgranular strain will decrease as well. However, after ageing for prolonged periods, solute supply to the grain boundary becomes exhausted because of matrix precipitation. In an effort to minimize their total surface free energy, the grain boundary phases start to coarsen, which will decrease the fractional area coverage of the grain boundary. An increase in local critical fracture strain and thus in bulk fracture strain will be the consequence. Therefore, the observed minimum in fracture strain for the air-cooled sample can be explained by the onset of coarsening of the grain boundary phases after a certain amount of ageing time. This description is further supported by experimentally measured cusp-size distributions resulting from void coalescence at the grain boundary, presented in Fig. 12. Only cusps from voids that formed at grain boundaries perpendicular to the applied load were considered, because for other grain boundary orientations the influence of shear on cusp-shape may be considerable. In the figure the effect of coarsening, which sets in after about 5 hrs of ageing judging from the fracture-strain diagram, is reflected in a shift of the cusp size distribution to larger sizes with ageing time from 5 hrs. The average critical void size at fracture increases in fact from 1.74 μm to 1.97 μm. After the increase in fracture strain due to coarsening of the grain boundary precipitates, it exhibits a next local maximum and decreases again after 23 hrs of ageing. This maximum may find its origin in coarsening of the matrix precipitates during over-ageing. Matrix slip will become more localized again, increasing the tendency for shear fracture. Also the amount of intergranular failure would normally have increased, but due to coarsening of grain boundary precipitates this effect is not so pronounced. The final decrease in fracture strain during over-ageing thus is mainly caused by the increased amount of shear.

As the percentage of intergranular failure is largest in the peak-aged condition for both water-quenched and air-cooled recrystallized product, the grain boundary properties can best be correlated to the bulk mechanical properties at this point. From Fig. 4, the bulk fracture strains after both cooling-rates can be seen to be about equal (∼15%) after 23 hrs of artificial ageing. As determined from the TEM-micrographs, the

precipitate-free-zone widths are 35 nm and 280 nm for the water-quenched and air-cooled alloys respectively. Using the grain boundary precipitation model described in [8], adapted for the AA6061 alloy, the volume fraction of grain boundary precipitates in the precipitate free zone in peak-aged condition was calculated to be ∼6.4% for the water-quenched alloy. As this model is based on non-equilibrium segregation conditions and as it considers segregation and precipitation as two separate processes, it may not be valid for the air-cooled case. Because a direct determination of grain boundary precipitate volume fraction in the precipitate-free-zone from TEM-micrographs is not very accurate, it is also derived from the average dimple size of the fracture surface. According to [9], a linear relationship between dimple size and particle spacing exists. The average dimple size after 23 hrs of ageing was found to be ∼2 μm in both orthogonal directions lying in the grain boundary plane, which would imply a particle spacing of ∼1 μm according to the above reference. This value is comparable to the observed interdistance in Fig. 9b. Together with the observed particle size, this corresponds to a grain boundary precipitate volume fraction (i.e., in the PFZ) of ∼4.5% for the air-cooled alloy. At first sight it may seem contradictory that this value is smaller than that for the water-quenched case, but it can be explained by the much wider PFZ for the air-cooled alloy. For the present volume fractions the critical strain for void nucleation ε_n is found to have a minor influence on the intergranular fracture strain ε_{fi} and it is assumed to be equal to the strain at yielding (i.e., 1.4% for both cases). As the precipitate volume fraction for the air-cooled alloy is smaller and since the PFZ-width is larger by a factor 8, the total fraction of strain localized to the grain boundary region is largest for the air-cooled alloy. From Equation 1, the PFZ-confined strains can be calculated to be equal to 61.7% and 89.5% for the water-quenched and air-cooled alloy respectively, which may explain the larger fraction of ductile intergranular fracture for the air-cooled alloy. Although these values may seem rather large, the corresponding elongations of the PFZ (0.02 μm and 0.25 μm) are very small because of its relative small width. If it is assumed that the bulk elongation is equally distributed over all grains (average grain size $D \sim 14$ μm) in the gage length (i.e., 20 mm), a total elongation per grain of ∼2.1 μm before fracture can be estimated for both cases. This elongation is distributed over one grain interior and two half-width PFZs on both sides. Comparing the values above, it can be seen that even for the air-cooled alloy at peak-strength, the elongation of the grain interior is still one order of magnitude larger than the elongation of the grain boundary region. The same holds for the strain. From Equation 2, it can be calculated that of the bulk fracture strain of 15%, the transgranular strains for water-quenched and air-cooled product respectively are 14.8% and 13.2%.

5.2. Comparison of recrystallized and extruded microstructure at peak-strength

From the stress-strain curves, the strengths of the extruded water-quenched and air-cooled samples were

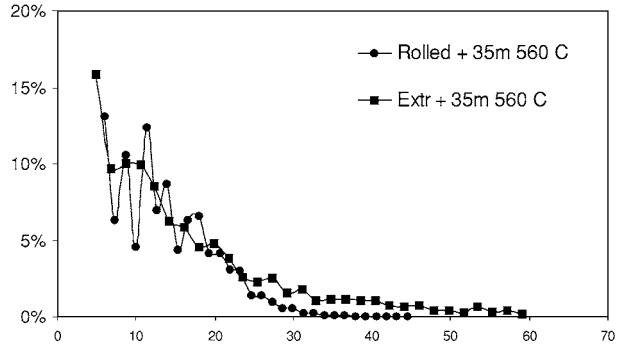

Figure 13 Grain size distributions (units of μm) of AA6061 with recrystallized- and extruded microstructure.

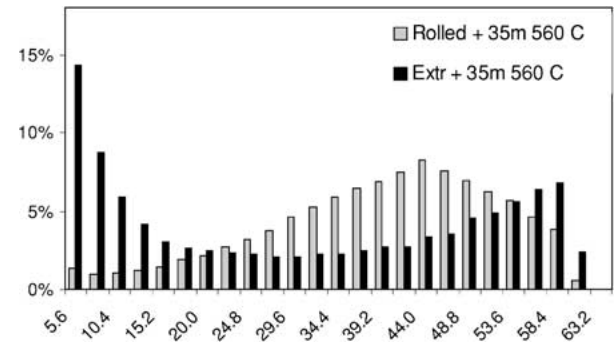

Figure 14 Grain boundary misorientation angle (in degrees) distributions of AA6061 with recrystallized- and extruded microstructures.

450 MPa and 400 MPa respectively, and are thus comparable to the peak-aged strengths of recrystallized material. On the other hand, the fracture strain of peak-aged extruded material is much smaller than that of recrystallized material; 8.6% and 4.3% for extruded water-quenched and air-cooled alloys respectively vs. ∼15% for the recrystallized alloy. As the grain size distribution is comparable for both microstructures (see Fig. 13), this cannot explain the observed difference in mechanical properties.

The smaller strain to fracture with respect to the recrystallized alloy may be explained by a much coarser distribution of intermetallic phases in the extruded microstructure. For the recrystallized microstructure, this distribution is more refined during cold-rolling. A finer distribution to a greater extent prevents localization of slip, so that the fracture mode will be more ductile in nature. Severe slip localization in the extruded alloy on the other hand, increases shear band formation as well as stresses ahead of the pile-ups acting on the grain boundary region, both reducing the fracture strain [10, 11]. Regarding the fracture surfaces of the extruded alloy (Fig. 8), it is clear that the fraction of intergranular failure for both water-quenched and air-cooled extruded alloy is significantly smaller than for the recrystallized alloy. This can be explained by the larger fraction of low-angle grain boundaries in extruded material, which is presented in Fig. 14. Segregation and precipitation at this type of boundaries are less pronounced, their precipitate-free zones are smaller (Fig. 9d), their cohesive strength is larger and slip transmission is easier. Plastic deformation thus will be less concentrated at these grain boundaries rendering a larger fraction of

transgranular fracture (predominantly shear fracture) for the extruded microstructure.

Considering fracture behaviour for the extruded microstructure subjected to different cooling rates, the fraction of intergranular fracture for the air-cooled alloy can be seen to be significantly larger than that for the water-quenched alloy. This may affect bulk fracture and may thus explain the large difference in fracture strain between the two alternative cooling-rates. The difference in fraction of intergranular failure between air-cooled and water-quenched material for the recrystallized microstructure at peak-strength is much smaller, and consequently the difference in fracture strains is also smaller.

6. Conclusions

Large grain boundary phases in the as-air-cooled alloy, may explain its much smaller fracture strain with respect to the water-quenched alloy. With increasing artificial ageing time, the bulk fracture strain of the air-cooled alloy exhibits a minimum. This can be explained by grain boundary precipitate growth and coarsening affecting the fraction of strain confined to the grain boundary region.

For the recrystallized microstructure aged to peak strength, the fraction of intergranular fracture is much larger for the air-cooled alloy. This can be understood on the basis of a much wider precipitate free zone and a smaller grain boundary precipitate volume fraction for the air-cooled alloy, increasing the fraction of strain confined to the grain boundary region by about one order of magnitude with respect to the water-quenched alloy.

A much coarser distribution of intermetallic phases in the extruded microstructure is responsible for a larger degree of slip localization. This enhances the tendency for shear- and intergranular fracture, reducing the ductility and thus the fracture strain with respect to that of the recrystallized microstructure.

Although slip localization is more pronounced, the larger amount of low-angle grain boundaries in extruded product decreases the fraction of ductile intergranular fracture for the air-cooled case significantly.

Acknowledgements

This research was carried out under projectnumber MS.97001A in the framework of the Strategic Research programme of the Netherlands Institute for Metals Research in the Netherlands

References

1. D. S. THOMPSON, *Metall. Trans.* **6A** (1975) 671.
2. B. MORERE, J. C. EHRSTRÖM and I. SINCLAIR, *ibid.* **31A** (2000) 2503.
3. L. M. BROWN and J. D. EMBURY, *Proc. 3rd ICSMA* **1** Cambridge (1973), Vol. 1, p. 164.
4. S. E. URRETA, F. LOUCHET and A. GHILARDUCCI, *Mat. Sci. Eng.* A **302** (2001) 300.
5. M. GRÄF and E. HORNBOGEN, *Acta Met.* **25** (1977) 883.
6. A. J. BRYANT and A. T. THOMAS, *J. Inst. Met.* **100** (1972) 40.
7. L. ZHEN, S. B. KANG and H. W. KIM, *Mater. Sci and Tech.* **13** (1997) 905.
8. H. JIANG and R. G. FAULKNER, *Acta Mater.* **44** (1996) 1857.
9. D. BROEK, *Enging. Fracture Mech.* **5** (1973) 55.
10. J. M. DOWLING and J. W. MARTIN, *Acta Metall.* **24** (1976) 1147.
11. J. A. BLIND and J. W. MARTIN, *Mat. Sci. Eng.* **57** (1983) 49.

Received 10 January
and accepted 16 August 2002